Synthesis and Optoelectronic Properties of Ultrathin Ga_2O_3 Nanowires

Eli Sutter,[1*] Juan Carlos Idrobo,[2] and Peter Sutter[3]
[1]Department of Mechanical & Materials Engineering, University of Nebraska-Lincoln, Lincoln NE 68588, United States
[2]Center for Nanophase Materials Sciences, Oak Ridge National Laboratory, Oak Ridge, TN 37831, United States
[3]Department of Electrical & Computer Engineering, University of Nebraska-Lincoln, Lincoln NE 68588, United States

Abstract

Gallium oxide (Ga_2O_3) and its most stable modification, monoclinic β-Ga_2O_3, is emerging as a primary material for power electronic devices, gas sensors and optical devices due to a high breakdown voltage, large bandgap, and optical transparency combined with electrical conductivity. Growth of β-Ga_2O_3 is challenging and most methods require very high temperatures. Nanowires of β-Ga_2O_3 have been investigated extensively as they might be advantageous for devices such as nanowire field effect transistors, gas sensors benefiting from a large surface to volume ratio, among others. Here, we report a synthesis approach using a sulfide precursor (Ga_2S_3), which requires relatively low substrate temperatures and short growth times to produce high-quality single crystalline β-Ga_2O_3 nanowires in high yields. Even though Au or Ag-rich nanoparticles are invariably observed at the nanowire tips, they merely serve as nucleation seeds while the nanowire growth proceeds *via* supply and local oxidation of gallium at the substrate interface. Absorption and cathodoluminescence spectroscopy on individual nanowires confirms a wide bandgap of 4.63 eV and strong luminescence with a maximum ~2.7 eV. Determining the growth process, morphology, composition and optoelectronic properties on the single nanowire level is key to further application of the β-Ga_2O_3 nanowires in electronic devices.

Keywords: Nanowires, gallium oxide, low loss EELS, cathodoluminescence.

*Corresponding author: esutter@unl.edu

INTRODUCTION

Gallium (III) oxide (Ga_2O_3) is currently attracting a lot of interest for use in electronics for low-loss high power switching[1] and in truly solar-blind UV photodetectors[2-3] that have a number of military and civil surveillance applications such as missile tracking, fire detection, and ozone hole monitoring.[4] Monoclinic β-Ga_2O_3, the most stable crystal modification, is a thermally and chemically stable wide bandgap semiconductor (E_g ~ 4.9 eV) with a very high predicted breakdown voltage, 8 MV/cm, close to that of diamond.[5] Ga_2O_3 shows also intense blue defect emission (446 nm (2.78 eV)) associated with a donor-acceptor pair (DAP) recombination mechanism, where the donor species are proposed to be oxygen vacancies and the acceptors gallium vacancies or gallium–oxygen vacancy pairs in the bulk.[6-9] Ga_2O_3 films are promising for ultra-low power loss, high-efficiency power applications[1] with high breakdown electric fields and on/off ratio above 10^4 (ref. [10]) as well as gas sensors.[11] Nanoscale Ga_2O_3 in the form of nanoribbons, flakes, nanorods, and nanowires (NWs) is of similar interest. Mechanically exfoliated Ga_2O_3 nanoribbons and flakes show promise for field effect transistors (FETs),[12] CO detectors,[13] deep UV photodetectors with high sensitivity, stability, signal-to-noise ratio, spectral selectivity, and fast time response up to temperatures above 430 K,[14] as well as emerging applications as multimode nanoresonators.[15] Ga_2O_3 nanorods loaded with Pd are promising supports for methanol production by CO_2 hydrogenation,[16] the synthesis of alkyl carbamates from CO_2 and n-propanol,[17] and photoelectrochemical water splitting.[18] Ga_2O_3 nanostructures also show promise for controlling doping, which has turned out notoriously hard in the bulk. Similar to the bulk, β-Ga_2O_3 nanowires generally exhibit n-type conductivity due to native oxygen vacancies,[19] but p-type doping[20-21] and p-n homojunctions have been successfully demonstrated for NWs. Remarkably, in addition to the strong blue defect luminescence,[22-23] intentionally nitrogen-doped Ga_2O_3 nanorods and nanowires also emit red light (600-800 nm),

thus becoming excellent white light emitters.[24]

Ga_2O_3 nanowires have been prepared by a variety of methods that invariably require very high temperatures, maintained for several hours due to low vapor pressures of the typical precursor powders. The synthesis methods include carbothermal reduction synthesis from gallium oxide powders with added graphite at 980°C,[22] with carbon nanotubes at 1100°C,[25] in the presence of carbon at 900-1000°C,[26,27] or with ZnO and graphite powders at 900°C;[20] atmospheric pressure CVD using Ga and water as precursors (850-950°C);[28] evaporation of GaN powder (1100°C) [29] and GaAs (750-900°C);[30] thermal evaporation of gallium oxide (1000-1200°C);[31] and Ga evaporation (800°C,[32] 700-1050°C,[6] 900°C,[33-34] 1300°C).[24] Even the use of organometallic precursors such as gallium acetylacetonate[35] and tBu_3Ga,[36] which decompose at relatively low temperatures requires very high substrate temperatures (550-850°C). [33,36,35, 37] The identification of an alternative precursor that could lower the growth temperature, and perhaps even more importantly the growth duration would significantly decrease the thermal budget of the sample associated with the synthesis and could enable the further development of non-equilibrium processes such as doping (to form high-quality junctions) or substitution (*e.g.*, incorporation of N for optoelectronics). Interestingly, many studies do not report any intentional source of oxygen other than, supposedly, "residual oxygen" in the growth system. The synthesis is, however, frequently performed on oxide substrates, such as Al_2O_3,[29,31] CeO_2,[30] and Si covered by its native oxide,[33-34] which could be reduced by the metal flux and release sufficient oxygen for the formation of Ga_2O_3 nanowires.

Here we report on the synthesis of ultrathin single crystalline Ga_2O_3 nanowires from a gallium (III) sulfide (Ga_2S_3) powder precursor at moderate substrate temperatures and source temperatures that are among the lowest reported for a solid precursor. Transmission electron

microscopy (TEM) and related methods are used to investigate the morphology and composition of the nanowires. We demonstrate that despite the use of Au and Ag catalysts and the presence of metal alloy particles at tips of the Ga_2O_3 nanowires, the wires likely do not form by a vapor-liquid-solid (VLS) process but rather *via* root growth involving an unconventional reduction of the SiO_2 substrate by the Ga precursor, confined at the nanowire-substrate interface. Optoelectronic measurements on individual Ga_2O_3 nanowires by nanoscale absorption and luminescence spectroscopy show an absorption edge (*i.e.*, fundamental bandgap) of 4.63 eV and bright luminescence with maximum at ~450 nm (*i.e.*, ~2.75 eV photon energy). These characteristics document the promising optoelectronic properties of single-crystalline Ga_2O_3 nanowires.

RESULTS AND DISCUSSION

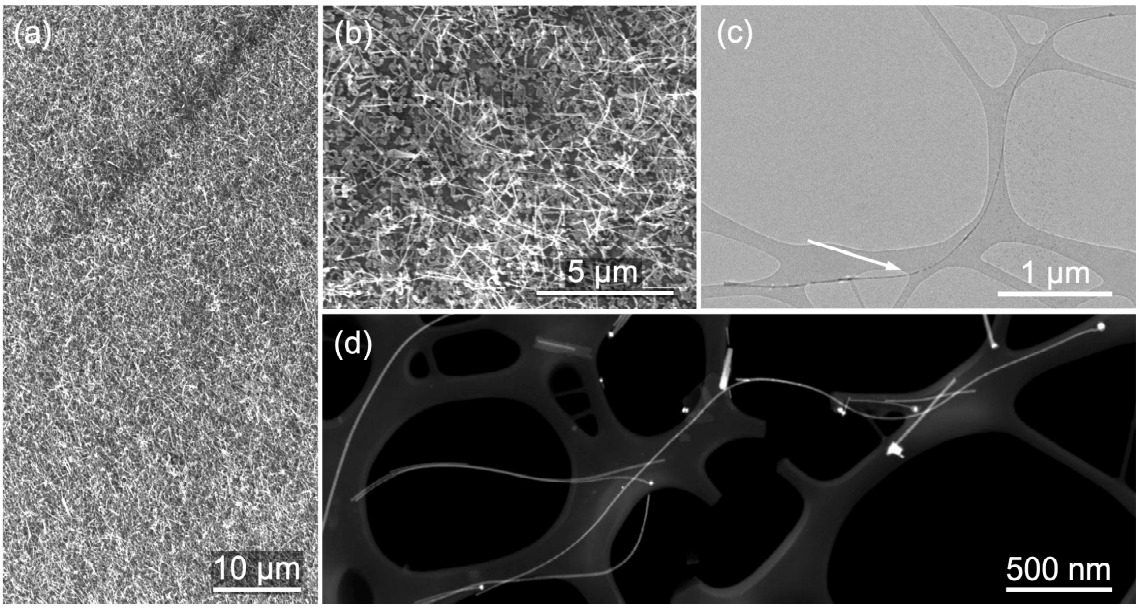

Figure 1. (a) Large-area SEM image of dense Ga_2O_3 nanowire forests grown on SiO_2 substrates covered with nominally 5 nm Ag film. **(b)** SEM image showing a detailed view of the sample in (a). **(c)** TEM of a Ga_2O_3 nanowire (arrow); **(d)** HAADF-STEM overview images of individual Ga_2O_3 NWs on amorphous carbon film (growth temperature: 550°C).

Ga_2O_3 nanowires were grown in the temperature range between 500-650°C, forming dense ensembles (~1 wire per 2 μm^2) on the oxidized Si substrates (thermal SiO_2, 300 nm) covered

with Au or Ag films with nominal thickness of 5 nm, as shown in the scanning electron microscopy (SEM) image in Figures 1 (a), (b). To investigate the structure and morphology at the level of individual Ga_2O_3 NWs, the wires were dispersed on carbon films supported by TEM copper grids. Figure 1 (c) and (d) show TEM and HAADF-STEM images of typical Ga_2O_3NWs grown at a temperature of 550°C. The NWs have diameters in the range between 10-30 nm and over a growth time of 20 minutes grow up to several tens of micrometers long.

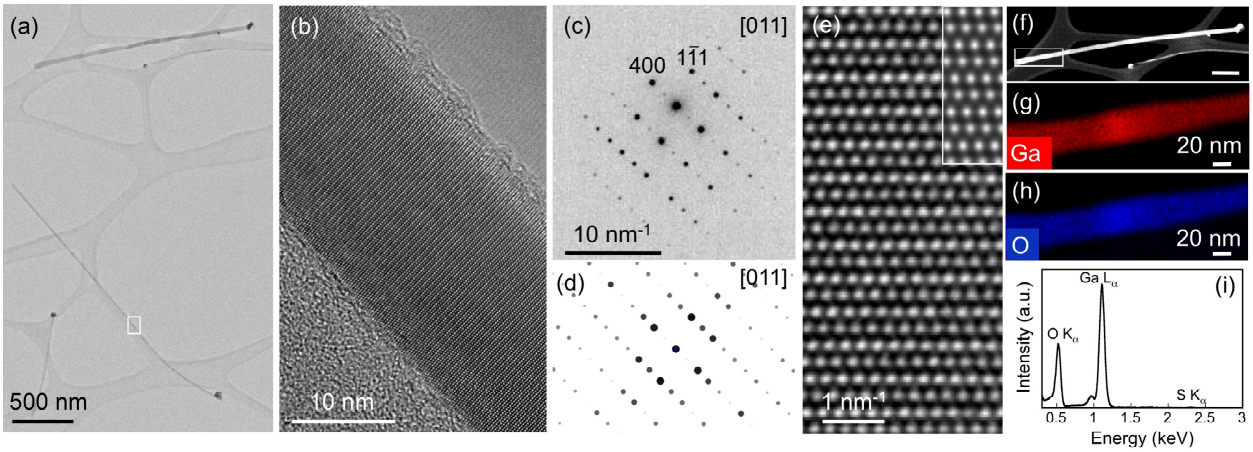

Figure 2. Morphology of single-crystalline Ga_2O_3 nanowires. (a) Overview TEM image of Ga_2O_3 nanowires on amorphous carbon film (growth temperature: 550°C). **(b)** High-resolution TEM image of the section of the Ga_2O_3 NW marked by a rectangle in (a). **(c)** Electron diffraction pattern of the Ga_2O_3 NW along the [011] zone axis. **(d)** Simulated electron diffraction pattern for monoclinic β-Ga_2O_3 along the [011] zone axis. **(e)** High-resolution TEM image of the β-Ga_2O_3 nanowire. Inset: Multislice image simulation. **(f)** HAADF-STEM image of representative Ga_2O_3 nanowires (scale bar: 200 nm). **(g) - (h)** EDS chemical maps of the Ga_2O_3 NW (area marked by a rectangle in (f)) showing the distribution of Ga (red) and oxygen (blue). **(i)** EDS spectrum from the nanowire.

Figures 2 (a) shows a TEM image of four characteristic Ga_2O_3 NWs on amorphous carbon support, illustrating the high aspect ratio and constant diameter of the NWs over extended distances. High-resolution TEM images (Figure 2 (b) and (e)) and electron diffraction patterns (Figure 2 (c)) demonstrate that the nanowires are high-quality single crystals. The electron diffraction pattern (Figure 2 (c)) can be indexed to the monoclinic β-Ga_2O_3 structure (a = 1.224 nm, b = 0.303, c = 0.579 nm)[38] along the [011] zone axis. The nanowire axis is oriented along the [100] direction.

Energy dispersive X-ray spectroscopy (EDS) chemical maps and spectra confirm that the NWs consist of Ga and O. The chemical maps show Ga and O uniformly distributed in the NWs (Figure 2 (g) – (h)). Quantification of EDS spectra confirms the Ga_2O_3 composition (Figure 2 (i)). It is worth noting that, despite the fact that the source is Ga_2S_3, the EDS spectra in Figure 2 (i) and Figure S4 show only very weak sulfur K_α signal in the nanowire.

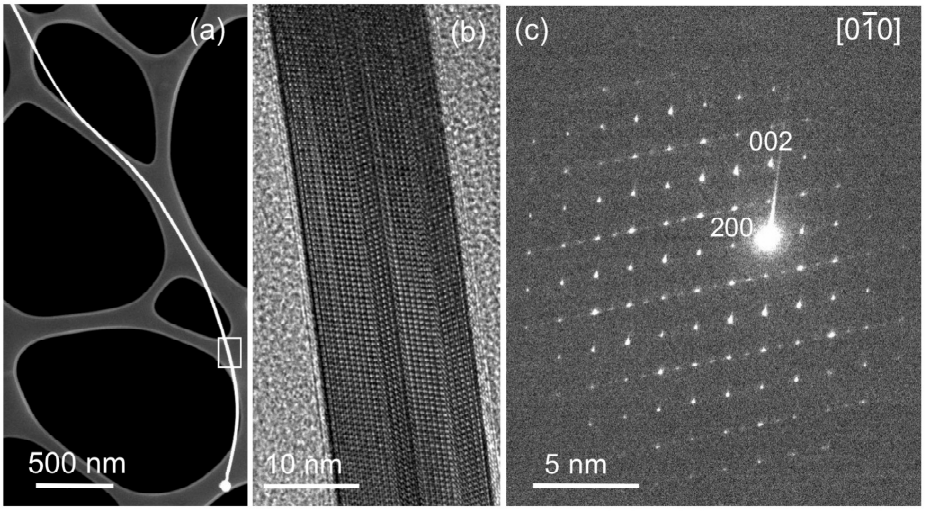

Figure 3. Morphology of single crystalline Ga_2O_3 nanowires grown on SiO_2/Si(100) substrate covered with nominally 2 nm Au film. **(a)** Overview STEM image of a Ga_2O_3 nanowire on amorphous carbon film (growth temperature: 550°C). **(b)** High-resolution TEM image of the section of the Ga_2O_3 NW marked by a rectangle in (a). **(c)** Electron diffraction pattern of the β-Ga_2O_3 NW along the [010] zone axis.

Analysis of electron diffraction patterns demonstrates that the β-Ga_2O_3 nanowires grown both on Au and Ag films have identical morphologies and orientation (Figure 3; Figures S1 and S2 – electron diffraction patterns of different NWs along the [010] zone axis). High-resolution TEM images show that, even though the β-Ga_2O_3 nanowires exhibit high crystal quality, they frequently incorporate isolated twins or sequences of twins (Fig. 3 (b)). The presence of twins can also be seen in the diffraction patterns, where additional spots appear on every second row along the [100] direction. Simulated electron diffraction patterns (Figure S1) show that these extra spots are indeed correlated with the appearance of twins. High-resolution TEM and electron diffraction confirm that not only the morphology of nanowires but also the propensity to

twinning is identical in β-Ga_2O_3 nanowires grown on Au (Figure 3 (c), Figure S1) and Ag (Figure S2).

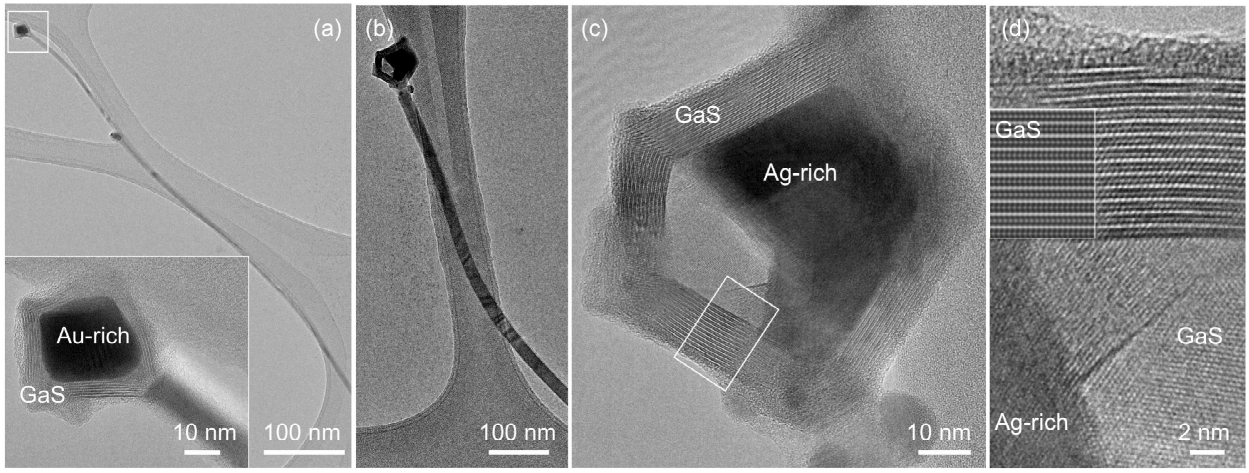

Figure 4. Representative TEM images obtained near the tips of Ga_2O_3 nanowires. (a) Overview TEM image of a typical Ga_2O_3 nanowire grown on SiO_2/Si(100) substrate covered with nominally 2 nm Au film (growth temperature: 500°C). **Inset**: High-resolution TEM image of the Au-rich tip, encapsulated in layered β-GaS. (**b)** Overview TEM image of the segment near the tip of a Ga_2O_3 nanowire grown on SiO_2/Si (100) substrate covered with nominally 2 nm Ag film (growth temperature: 550°C). **(c)** High-resolution TEM image of the Ag-rich tip encapsulated in a multilayer β-GaS shell. **(d)** High-resolution TEM image of the area marked by white rectangle in (c). Inset: Multislice image simulation showing an excellent match to the β-GaS structure.

Figure 4 shows TEM images of β-Ga_2O_3 nanowires close to their tips. While the NWs show uniform thickness and homogeneous composition along their lengths, the tips of the nanowires have a complex core-shell morphology. Electron diffraction and TEM imaging identify the shells to be crystalline layered β-GaS (hexagonal, space group $P6_3/mmc$, a = 3.587 Å, c = 15.492 Å).[39] High-resolution TEM imaging (Figure 4 (c), (d)) shows the characteristic atomic structure of the layered GaS stacked along the *c*-axis (zone axis, ZA: [100]) wrapped around the Ag-rich core (see below). Lattice fringes with a separation of 0.775 nm in the shell are consistent with the spacing of (0002) basal planes in layered bulk GaS.[39] The number of GaS monolayers, each consisting of two gallium and two sulfur planes in the sequence S–Ga–Ga–S, differs depending on the composition of the particle in the core and is usually ~ 2 monolayers for Au (Figure 4 (a) and S5) and 4-5 monolayers around Ag cores (Figure 4 (b)-(d)). Elemental maps and spectra

confirm the presence of Ga and O along the NWs (Figure 5 (b) – (c)). The cores of the core-shell particles at the tip show dark contrast in TEM and bright Z-contrast in HAADF-STEM, consistent with the presence of high atomic number (Z) elements (Au, Ag). Indeed, EDS maps and spectra (Figure 5) of the bright high-Z regions show that the NW tip core contains Ag (or Au). The shell consists predominantly of Ga and S (Figure 5 (d) – (e)), consistent with the structure of GaS identified in Figure 4 (d). Thus, the chemical characterization confirms that the nanowire tips are silver- or gold-gallium-sulfide core-shell structures.

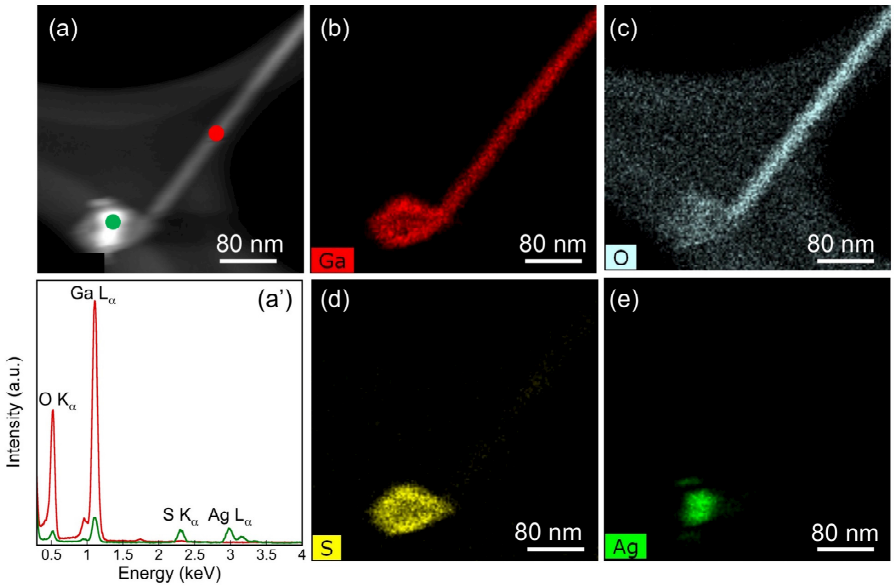

Figure 5. Composition of Ga_2O_3 nanowires near the tips. (a) HAADF-STEM image of a representative Ga_2O_3 nanowire, grown on SiO_2/Si covered with nominally 5 nm Ag, near the Ag-rich tip. **(b) - (e)** EDS chemical maps of the Ga_2O_3 NW showing the distribution of Ga (red), O (light blue), S (yellow) and Ag (green). **(a')** EDS spectra from the NW (red) and the tip (green), measured at the positions shown in (a).

The presence of metal alloy nanoparticles at nanowire tips is usually cited as evidence for catalyst-assisted growth of semiconductor NWs *via* a vapor-liquid-solid (VLS) process.[40] An unambiguous identification of this growth mechanism is provided by in-situ observations of NW growth.[41] The VLS growth involves metal-semiconductor binary[42] or pseudo-binary[43-44] alloy melt drops as growth seeds, whose interface to the semiconductor wire represents the NW growth front. The growth proceeds *via* adsorption on the alloy drop, diffusion through the liquid

and incorporation of new material at the catalyst drop-nanowire interface. In this process, the growing nanowire lifts the drop off the substrate and carries it along at the tip (tip growth). As the temperature is lowered upon termination of the growth, the solubility of the semiconducting material in the molten alloy drop decreases so that it is expelled and incorporated into the crystalline nanowire while the metal nanoparticle solidifies at the tip.[45]

At first glance, therefore, our observations of particles at the tips of the Ga_2O_3 NWs suggest that the growth follows VLS tip growth. However, several findings lead us to a different conclusion. During evaporation of Ga_2S_3, the precursor used here (Figure S3), the vapor consists predominantly of Ga_2S.[46] Even though the incorporation of Ga_2S into the drop should lead to supersaturation and growth of a GaS nanowire, growth of gallium sulfide nanowires is not observed. Following the growth process, the particles at the tips of the nanowires show complex core-shell morphologies consisting of metal (Au, Ag) rich cores and GaS shells (Figure 4). This finding suggests that the Ga_2S evaporated from the precursor is indeed incorporated in the Ag (Au) nanoparticles, in an amount determined by the corresponding alloy phase diagram at the growth temperature. The GaS shells of the nanowire tips are not structurally attached to the Ga_2O_3 nanowire, but appear to have phase separated from the alloy particle upon lowering the solubility during cooldown (Figure 4). Furthermore, the concentration of oxygen in the tips is much smaller than in the nanowires (Figure 5). Thus, we conclude that the alloy particles at the nanowire tips likely do not represent VLS growth catalysts for the growth of the Ga_2O_3 NWs, but merely participate in the initial nucleation after which they are lifted off the surface by the growing nanowires and no longer play an active role.

Growth of Ga_2O_3 requires sources of gallium, here in the form of Ga_2S vapor, and oxygen. While others have suggested residual gas in the growth reactor as the primary source of oxygen, the

amount of residual O_2 is expected to be minimal here since the vapor transport carrier gas is a mixture of dry Ar with 2% H_2 added to maintain a reducing atmosphere (see Methods for details). In addition, the evaporation of Ga_2S from the Ga_2S_3 precursor releases sulfur, which is well-known to counteract oxidation.[47] We also find that while the length of Ga_2O_3 NWs increases with growth time, their diameters remain constant, unlike observations for growth from metallic Ga with an added oxygen source (H_2O).[28] This points to a different source of oxygen, as well as a localization of the Ga-oxidation reaction. Consideration of the underlying thermodynamics shows that oxygen can be supplied by the SiO_2 substrate,[48] possibly aided by a re-supply *via* residual oxygen-containing species from the gas phase. At all temperatures the Gibbs free energy of formation of Ga_2O_3 (-998.3 kJ/mol at room temperature; -850 kJ/mol at 650°C)[49] is more negative than that of SiO and SiO_2 (-856.3 kJ/mol at room temperature; -705 kJ/mol at 650°C).[50-52] Thus SiO_2 can be reduced by Ga, resulting in the formation of Ga_2O_3. In addition, a small flux of Ga (or Ga sulfide vapor) could accelerate the process, similar to the low-temperature (non self-limiting) solid-state reaction $3\ SiO_2 + 4\ Al \rightarrow 2\ Al_2O_3 + 3\ Si$, which causes the parasitic transformation of SiO_2 to Al_2O_3 in devices where Al is in contact with a gate oxide.[53] This effect might be further enhanced at the nanometer-scale junction between the growing nanowire and the substrate similar to the preferential oxidation of In, which is accelerated tenfold at the interface between a Si nanowire and an In catalyst at its tip compared to oxidation at the indium-gas interface,[54] or enhanced Si oxidation due to the curvature of SiGe alloy nanowires, producing Ge nanowires encapsulated in SiO_2 shells.[48] Together with the factors discussed above, an oxidation mechanism involving the interface to the SiO_2 substrate strongly suggests that the β-Ga_2O_3 are formed by root growth with continuous deposition of Ga from the vapor phase and oxidation at the base. This implies that Ag or Au catalyst particles at

the nanowire tips play only a minor role, likely at the onset of nanowire growth where they can define the footprint of the wire. This growth mechanism is consistent with the observed constant nanowire diameter and fixed oxygen content. Close inspection of the literature lends additional support for this scenario. Indeed, several reports of Ga_2O_3 nanowire growth do not use an explicit source of oxygen but involve oxide substrates.[29-31, 33-34]

While these factors strongly support a root growth mechanism, a conventional VLS tip growth cannot be completely ruled out on the basis of our post-growth characterization. We therefore briefly discuss this alternative scenario. In tip growth, the Ag (or Au) rich drops at the nanowire tips would need to continuously absorb Ga_2S from the vapor phase to maintain a supersaturation of Ga in the catalysts, and require the desorption of excess sulfur to keep a stable stoichiometry while supplying Ga for Ga_2O_3 nanowire growth. The supply of oxygen would need to come entirely from the gas phase (where it should not be abundant, see Methods), *e.g.*, via adsorption on the catalyst surface and reaction at the interface to the growing wire.[54] Figure 4 shows that both Au and Ag catalysts contains sufficient Ga and S to crystallize multilayer GaS shells at the end of the growth. To be consistent with these morphologies, the conclusion of a tip growth process would then require a cooldown sequence in which excess Ga from the catalyst is first oxidized and incorporated into the Ga_2O_3 nanowire, followed by a phase separation of Ga and S to produce the observed crystalline GaS shells.

Single crystalline β-Ga_2O_3 nanowires are of interest for applications in optoelectronics, for example as solar blind photo detectors. In contrast to the traditional approaches to investigating the properties of the NWs *via* ensemble measurements such as optical absorption or photoluminescence (PL), we probed the optoelectronic properties using absorption and luminescence measurements on individual high-quality β-Ga_2O_3 nanowires. To obtain the

required nanometer-scale spatial resolution, we used high-resolution electron energy-loss spectroscopy (EELS) in aberration-corrected, monochromated STEM for single-nanowire absorption measurements and cathodoluminescence spectroscopy in STEM (STEM-CL) to probe light emission from individual wires. Figure 6 summarizes these measurements of the optoelectronic properties of our single crystalline β-Ga_2O_3 nanowires. Single-nanowire absorption measurements by EELS (Figure 6 (a)-(b)) show a characteristic energy loss onset associated with interband transitions across the fundamental bandgap at E_g = 4.63 eV, close to the previously reported bandgap of β-Ga_2O_3.[3, 37, 55-57] STEM-CL (Figure 6 (d) and (f)) shows intense luminescence from β-Ga_2O_3 nanowires (Figure 6 (c) and (e)). In comparison, the luminescence from the Au-GaS core-shell tip of the nanowires is much weaker. CL spectra (Figure 6 (f), inset) show a wide peak with maximum at a wavelength λ ~ 450 nm covering most of the visible spectrum, similar to the broad photoluminescence spectra measured on β-Ga_2O_3 nanowire ensembles at room temperature.[58] Note that our STEM-CL setup allows measurements

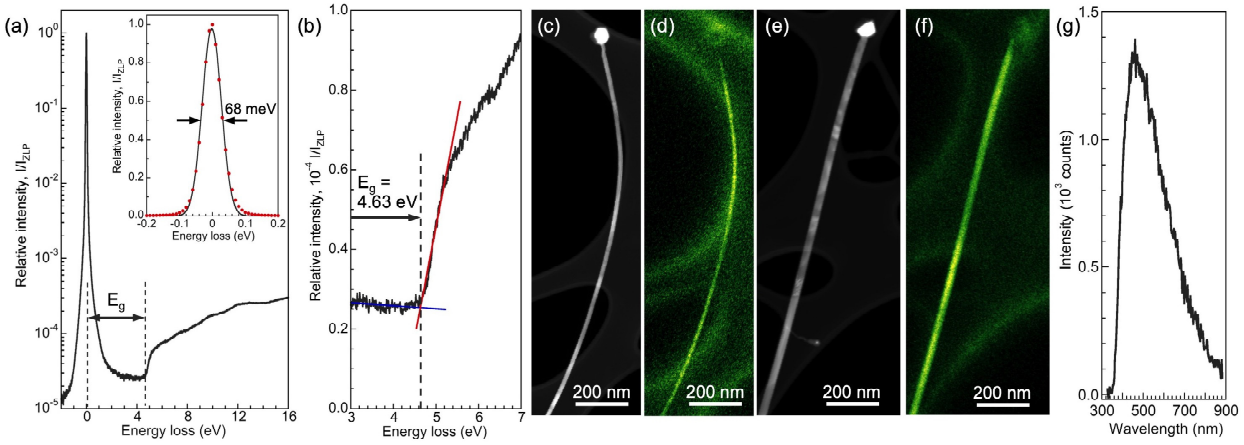

Figure 6. Optoelectronics of individual Ga_2O_3 nanowires. (a) Monochromated STEM-EEL spectrum providing a measurement (equivalent to optical absorption) of the bandgap (E_g) of a β-Ga_2O_3 nanowire. Inset: Gaussian fit to the zero-loss peak (ZLP), showing a full-width at half maximum of 68 meV. **(b)** Magnified view of the onset of interband losses in the EEL spectrum, showing a sharp onset at the fundamental bandgap E_g = 4.63 eV. **(c)-(g) STEM cathodoluminescence. (c), (e)** HAADF-STEM images of two β-Ga_2O_3 nanowires. **(d), (f)** Corresponding panchromatic STEM-CL maps, showing predominant photon emission from the Ga_2O_3 nanowires and only weak emission from the tip. **(g)** CL spectrum from the NW in (c), (d).

across the visible spectrum (350 - 950 nm), *i.e.*, cannot access luminescence across the fundamental bandgap of β-Ga_2O_3. Nevertheless, the nanowires show intense luminescence, whose origin is likely defect related and may involve DAP recombination found to give rise to similar bright blue emission (λ = 446 nm) both in bulk β-Ga_2O_3[6-9] and in β-Ga_2O_3 nanowires.[22-23]

CONCLUSIONS

In summary, we demonstrated the synthesis of high-quality single crystalline β-Ga_2O_3 nanowires in a relatively low-temperature process with reduced sample thermal budget based on a Ga_2S_3 precursor. The ultrathin nanowires reach several tens of microns in length over short growth times of the order of minutes. We identify the crystal structure and composition of the nanowires as β-Ga_2O_3 with propensity toward twin formation. Investigation of the nanoparticles at the tips of the nanowires demonstrates complex core-shell Au(Ag)-layered gallium sulfide (GaS) morphology, suggesting that even though the particles define the position of the growing gallium oxide nanowires they do not participate actively in their growth. Instead, nanowire growth appears to involve a root process in which the oxidation of Ga, delivered from the sulfide precursor, occurs at the nanoscale interface to the oxide (SiO_2) substrate, which is locally reduced in the process. EEL and cathodoluminescence spectroscopy on individual nanowires show their optoelectronic properties, notably a ~4.63 eV bandgap and intense defect emission due to the inherent defect structure of Ga_2O_3.

MATERIALS AND METHODS

Ga_2O_3 nanowires were synthesized by thermal evaporation from a Ga_2S_3 powder precursor (99.99%, ProChem, Inc.) in a quartz tube reactor heated by a furnace with two independently controlled temperature zones. After loading the substrates and powder precursor, the reactor was

pumped to below 10^{-3} Torr and purged for at least 30 minutes with the Ar:H_2 carrier gas mixture. The purging process was continued during the temperature ramp-up of the furnace (1 hour), thus ensuring the thermal desorption of adsorbates from the hot interior walls and surfaces of the reactor. The evaporation zone containing a quartz boat with the Ga_2S_3 powder was heated to 850°C. The zone containing the substrate was heated to growth temperatures T_s of 500-600°C. To ensure a constant temperature during the reaction, the two furnace zones were ramped so as to reach the chosen settings at the same time. Si wafers with 300 nm thermal SiO_2, covered with nominally 2-5 nm thick Ag or Au films deposited by magnetron sputtering at room temperature were used as substrates. The thin Au or Ag films dewet at the growth temperature to form polydisperse nanoparticle ensembles.[59-60] Over this Au (Ag) nominal thickness range, no significant changes in nanowire properties (thickness, density, *etc.*) were noticeable. During growth a Ar:H_2 (2%) carrier gas flow (research grade, 99.9999% purity) was maintained at 60 standard cubic centimeters per minute (sccm) and a pressure of 20 mTorr. The typical growth duration was 20 minutes. Upon completion of each growth, the reactor naturally cooled to room temperature.

The morphology of the Ga_2O_3 nanowires was investigated by TEM, HAADF-STEM, and nanobeam electron diffraction in an FEI Talos F200X field-emission microscope. For these investigations the nanowires were contact dry-transferred and dispersed on amorphous C films supported by Cu grids. The optoelectronic properties of individual Ga_2O_3 nanowires were investigated by both local absorption and luminescence spectroscopy. Absorption was measured by valence electron energy-loss spectroscopy in a monochromated aberration-corrected STEM (Nion Hermes at Oak Ridge National Laboratory) operated at 60 kV. Cathodoluminescence (CL) measurements were performed in the FEI Talos microscope (at the University of Nebraska) in

STEM mode (STEM-CL) using a Gatan Vulcan CL holder at room temperature and 200 keV electron energy. The incident beam current for STEM-CL measurements was typically 300-400 pA. Local CL spectra were acquired by positioning the electron beam at chosen locations and integrating the spectrometer output detected by a Si CCD array detector for 10-20 seconds.

ACKNOWLEDGEMENTS

This work was supported by the National Science Foundation, Division of Materials Research, Solid State and Materials Chemistry Program under Grant No. DMR-1904843. The monochromated EELS was supported by the Center for Nanophase Materials Sciences, which is a DOE Office of Science User Facility, using instrumentation within ORNL's Materials Characterization Core provided by UT-Batelle, LLC under Contract No. DE-AC05-00OR22725 with the U.S. Department of Energy and sponsored by the Laboratory Directed Research and Development Program of Oak Ridge National Laboratory, managed by UT-Battelle, LLC, for the U.S. Department of Energy. The authors would like to thank J. French for technical support.

References:

1. Chabak, K. D.; Leedy, K. D.; Green, A. J.; Mou, S.; Neal, A. T.; Asel, T.; Heller, E. R.; Hendricks, N. S.; Liddy, K.; Crespo, A.; Miller, N. C.; Lindquist, M. T.; Moser, N. A.; Fitch, R. C.; Walker, D. E.; Dorsey, D. L.; Jessen, G. H., Lateral β-Ga2O3 field effect transistors. *Semiconductor Science and Technology* **2019,** *35* (1), 013002.
2. Chen, X.; Ren, F.-F.; Ye, J.; Gu, S., Gallium oxide-based solar-blind ultraviolet photodetectors. *Semiconductor Science and Technology* **2020,** *35* (2), 023001.
3. Pearton, S. J.; Yang, J.; CaryIV, P. H.; Ren, F.; Kim, J.; Tadjer, M. J.; Mastro, M. A., A review of Ga2O3 materials, processing, and devices. *Applied Physics Reviews* **2018,** *5* (1), 011301.
4. Guo, D.; Guo, Q.; Chen, Z.; Wu, Z.; Li, P.; Tang, W., Review of Ga2O3-based optoelectronic devices. *Materials Today Physics* **2019,** *11*, 100157.
5. Higashiwaki, M.; Sasaki, K.; Kuramata, A.; Masui, T.; Yamakoshi, S., Development of gallium oxide power devices. *physica status solidi (a)* **2014,** *211* (1), 21-26.
6. Hosein, I. D.; Hegde, M.; Jones, P. D.; Chirmanov, V.; Radovanovic, P. V., Evolution of the faceting, morphology and aspect ratio of gallium oxide nanowires grown by vapor–solid deposition. *Journal of Crystal Growth* **2014,** *396*, 24-32.
7. Binet, L.; Gourier, D., ORIGIN OF THE BLUE LUMINESCENCE OF β-Ga2O3. *Journal of Physics and Chemistry of Solids* **1998,** *59* (8), 1241-1249.
8. Harwig, T.; Kellendonk, F., Some observations on the photoluminescence of doped β-galliumsesquioxide. *Journal of Solid State Chemistry* **1978,** *24* (3), 255-263.
9. Kumar, M.; Kumar, S.; Kumar, V.; Singh, R., 5 - Growth, properties, and applications of β-Ga2O3 nanostructures. In *Gallium Oxide*, Pearton, S.; Ren, F.; Mastro, M., Eds. Elsevier: 2019; pp 91-115.
10. Yan, X.; Esqueda, I. S.; Ma, J.; Tice, J.; Wang, H., High breakdown electric field in β-Ga2O3/graphene vertical barristor heterostructure. *Applied Physics Letters* **2018,** *112* (3), 032101.
11. Binions, R.; Carmalt, C. J.; Parkin, I. P.; Pratt, K. F. E.; Shaw, G. A., Gallium Oxide Thin Films from the Atmospheric Pressure Chemical Vapor Deposition Reaction of Gallium Trichloride and Methanol. *Chemistry of Materials* **2004,** *16* (12), 2489-2493.
12. Ahn, S.; et al., Effect of front and back gates on β-Ga2O3 nano-belt field-effect transistors. *Appl. Phys. Lett.* **2016,** *109*.
13. Yan, S.; Wan, L.; Li, Z.; Zhou, Y.; Zou, Z., Synthesis of a mesoporous single crystal Ga2O3 nanoplate with improved photoluminescence and high sensitivity in detecting CO. *Chemical Communications* **2010,** *46* (34), 6388-6390.
14. Zou, R.; Zhang, Z.; Liu, Q.; Hu, J.; Sang, L.; Liao, M.; Zhang, W., High Detectivity Solar-Blind High-Temperature Deep-Ultraviolet Photodetector Based on Multi-Layered (l00) Facet-Oriented β-Ga2O3 Nanobelts. *Small* **2014,** *10* (9), 1848-1856.
15. Zheng, X.-Q.; Lee, J.; Rafique, S.; Han, L.; Zorman, C. A.; Zhao, H.; Feng, P. X. L., Ultrawide Band Gap β-Ga2O3 Nanomechanical Resonators with Spatially Visualized Multimode Motion. *ACS Applied Materials & Interfaces* **2017,** *9* (49), 43090-43097.
16. Qu, J.; Zhou, X.; Xu, F.; Gong, X.-Q.; Tsang, S. C. E., Shape Effect of Pd-Promoted Ga2O3 Nanocatalysts for Methanol Synthesis by CO2 Hydrogenation. *The Journal of Physical Chemistry C* **2014,** *118* (42), 24452-24466.
17. Shah, J.; Ratnasamy, P.; Carreon, M. L., Influence of the Nanostructure of Gallium Oxide Catalysts on Conversion in the Green Synthesis of Carbamates. *Catalysts* **2017,** *7* (12), 372.

18. He, W.; Wu, W.; Li, Q.; Chen, K.; Lu, X., Facile Fabrication of Ga2O3 Nanorods for Photoelectrochemical Water Splitting. *ChemNanoMat* **2020,** *6* (2), 208-211.
19. Kumar, S.; Singh, R., Nanofunctional gallium oxide (Ga2O3) nanowires/nanostructures and their applications in nanodevices. *physica status solidi (RRL) – Rapid Research Letters* **2013,** *7* (10), 781-792.
20. Feng, Q.; Liu, J.; Yang, Y.; Pan, D.; Xing, Y.; Shi, X.; Xia, X.; Liang, H., Catalytic growth and characterization of single crystalline Zn doped p-type β-Ga2O3 nanowires. *Journal of Alloys and Compounds* **2016,** *687*, 964-968.
21. Liu, L. L.; Li, M. K.; Yu, D. Q.; Zhang, J.; Zhang, H.; Qian, C.; Yang, Z., Fabrication and characteristics of N-doped β-Ga2O3 nanowires. *Applied Physics A* **2010,** *98* (4), 831-835.
22. Wu, X. C.; Song, W. H.; Huang, W. D.; Pu, M. H.; Zhao, B.; Sun, Y. P.; Du, J. J., Crystalline gallium oxide nanowires: intensive blue light emitters. *Chemical Physics Letters* **2000,** *328* (1), 5-9.
23. Tien, L.-C.; Ho, C.-H., 4 - Synthesis, optical characterization, and environmental applications of β-Ga2O3 nanowires. In *Gallium Oxide*, Pearton, S.; Ren, F.; Mastro, M., Eds. Elsevier: 2019; pp 67-90.
24. Vanithakumari, S. C.; Nanda, K. K., A One-Step Method for the Growth of Ga2O3-Nanorod-Based White-Light-Emitting Phosphors. *Advanced Materials* **2009,** *21* (35), 3581-3584.
25. Gundiah, G.; Govindaraj, A.; Rao, C. N. R., Nanowires, nanobelts and related nanostructures of Ga2O3. *Chemical Physics Letters* **2002,** *351* (3), 189-194.
26. Li, J.; Wang, L.-S.; Buchholz, D. B.; Chang, R. P. H., Simultaneous Growth of Pure Hyperbranched Zn3As2 Structures and Long Ga2O3 Nanowires. *Nano Letters* **2009,** *9* (5), 1764-1769.
27. Cho, K. K.; Cho, G. B.; Kim, K. W.; Ryu, K. S., Growth behavior of β-Ga2O3nanomaterials synthesized by catalyst-free thermal evaporation. *Physica Scripta* **2010,** *T139*, 014079.
28. Terasako, T.; Kawasaki, Y.; Yagi, M., Growth and morphology control of β-Ga2O3 nanostructures by atmospheric-pressure CVD. *Thin Solid Films* **2016,** *620*, 23-29.
29. Dai, Z. R.; Pan, Z. W.; Wang, Z. L., Gallium Oxide Nanoribbons and Nanosheets. *The Journal of Physical Chemistry B* **2002,** *106* (5), 902-904.
30. Wang, H.; Wang, Y.; Gong, S.; Zhou, X.; Yang, Z.; Yang, J.; Han, N.; Chen, Y., Growth of Ga2O3 Nanowires via Cu-As-Ga Ternary Phase Diagram. *Crystals* **2019,** *9* (3), 155.
31. Chun, H. J.; Choi, Y. S.; Bae, S. Y.; Seo, H. W.; Hong, S. J.; Park, J.; Yang, H., Controlled Structure of Gallium Oxide Nanowires. *The Journal of Physical Chemistry B* **2003,** *107* (34), 9042-9046.
32. Sinha, G.; Datta, A.; Panda, S. K.; Chavan, P. G.; More, M. A.; Joag, D. S.; Patra, A., Self-catalytic growth and field-emission properties of Ga2O3nanowires. *Journal of Physics D: Applied Physics* **2009,** *42* (18), 185409.
33. Othonos, A.; Zervos, M.; Christofides, C., Carrier dynamics in β-Ga2O3 nanowires. *Journal of Applied Physics* **2010,** *108* (12), 124302.
34. Alhalaili, B.; Vidu, R.; Islam, M. S., The Growth of Ga2O3 Nanowires on Silicon for Ultraviolet Photodetector. **2019,** *19*, 5301.
35. Chang, K.-W.; Wu, J.-J., Low-Temperature Catalytic Growth of β-Ga2O3 Nanowires Using Single Organometallic Precursor. *The Journal of Physical Chemistry B* **2004,** *108* (6), 1838-1843.

36. Schulz, S.; Bendt, G.; Assenmacher, W.; Sager, D.; Bacher, G., Low-Temperature MOCVD of Crystalline Ga2O3 Nanowires using tBu3Ga. *Chemical Vapor Deposition* **2013,** *19* (10-11-12), 347-354.
37. Wang, G.; Park, J.; Kong, X.; Wilson, P. R.; Chen, Z.; Ahn, J.-h., Facile Synthesis and Characterization of Gallium Oxide (β-Ga 2O 3) 1D Nanostructures: Nanowires, Nanoribbons, and Nanosheets. *Crystal Growth & Design* **2008,** *8* (6), 1940-1944.
38. Ahman, J.; Svensson, G.; Albertsson, J., A Reinvestigation of [beta]-Gallium Oxide. *Acta Crystallographica Section C* **1996,** *52* (6), 1336-1338.
39. Pardo, M. P.; Guittard, M.; Chilouet, A.; Tomas, A., Diagramme de phases gallium-soufre et études structurales des phases solides. *Journal of Solid State Chemistry* **1993,** *102* (2), 423-433.
40. Sutter, E.; Sutter, P., Phase Diagram of Nanoscale Alloy Particles Used for Vapor−Liquid−Solid Growth of Semiconductor Nanowires. *Nano Letters* **2008,** *8* (2), 411-414.
41. Kodambaka, S.; Tersoff, J.; Reuter, M. C.; Ross, F. M., Germanium Nanowire Growth Below the Eutectic Temperature. *Science* **2007,** *316* (5825), 729-732.
42. Sutter, P. W.; Sutter, E. A., Dispensing and surface-induced crystallization of zeptolitre liquid metal-alloy drops. *Nat Mater* **2007,** *6* (5), 363-366.
43. Sutter, P.; Wimer, S.; Sutter, E., Chiral twisted van der Waals nanowires. *Nature* **2019,** *570* (7761), 354-357.
44. Sutter, E.; Sutter, P., 1D Wires of 2D Layered Materials: Germanium Sulfide Nanowires as Efficient Light Emitters. *ACS Applied Nano Materials* **2018,** *1* (3), 1042-1049.
45. Sutter, E. A.; Sutter, P. W., Size-Dependent Phase Diagram of Nanoscale Alloy Drops Used in Vapor−Liquid−Solid Growth of Semiconductor Nanowires. *ACS Nano* **2010,** *4* (8), 4943-4947.
46. Mills, K. C., *Thermodynamic Data for Inorganic Sulphides, Selenides and Tellurides*. Butterworths: London, 1974.
47. Keiser, C.; Sutter, P.; Sutter, E., Formation of Ge–GeS core–shell nanostructures via solid-state sulfurization of Ge nanowires. *CrystEngComm* **2018,** *20* (15), 2193-2200.
48. Sutter, E.; Camino, F.; Sutter, P., One-step synthesis of Ge–SiO2 core-shell nanowires. *Applied Physics Letters* **2009,** *94* (8), 083109.
49. Zinkevich, M.; Aldinger, F., Thermodynamic Assessment of the Gallium-Oxygen System. *Journal of the American Ceramic Society* **2004,** *87* (4), 683-691.
50. Olesinski, R. W.; Abbaschian, G. J., The Ge−Si (Germanium-Silicon) system. *Bulletin of Alloy Phase Diagrams* **1984,** *5* (2), 180-183.
51. Rao, P.; Kumar, S.; Reddy, G. L. N.; Veena, S.; Kalavathi, S.; Ramana, J. V.; Raju, V. S., Incorporation of oxygen during oxidative annealing of thermally evaporated In films. *Nuclear Instruments and Methods in Physics Research B* **2010,** *268*, 3395-3402.
52. Kolluri, S. V.; Chandorkar, A. N., Effect of Annealing on the Surface and Interface Properties of Indium Oxide Silicon Structures. *Thin Solid Films* **1993,** *230* (1), 39-44.
53. Dadabhai, F.; Gaspari, F.; Zukotynski, S.; Bland, C., Reduction of silicon dioxide by aluminum in metal–oxide–semiconductor structures. *Journal of Applied Physics* **1996,** *80* (11), 6505-6509.
54. Sutter, E.; Sutter, P., Enhanced oxidation of nanoscale In particles at the interface with a Si nanowire. *Applied Physics Letters* **2012,** *100* (23), 231602.

55. Chmielewski, A.; Moradifar, P.; Miao, L.; Lopez, K. A.; Zhang, Y.; Mauze, A.; Speck, J. S.; Alem, N., Investigation of the Atomic and Electronic Structure of β-(Al0.2Ga0.8)2O3 Alloys by STEM-EELS. *Microscopy and Microanalysis* **2019,** *25* (S2), 2186-2187.
56. Hwang, W. S.; Verma, A.; Peelaers, H.; Protasenko, V.; Rouvimov, S.; Xing, H.; Seabaugh, A.; Haensch, W.; Walle, C. V. d.; Galazka, Z.; Albrecht, M.; Fornari, R.; Jena, D., High-voltage field effect transistors with wide-bandgap β-Ga2O3 nanomembranes. *Appl Phys Lett* **2014,** *104* (20), 203111.
57. Orita, M.; Ohta, H.; Hirano, M.; Hosono, H., Deep-ultraviolet transparent conductive β-Ga2O3 thin films. *Appl Phys Lett* **2000,** *77* (25), 4166-4168.
58. Song, Y. P.; Zhang, H. Z.; Lin, C.; Zhu, Y. W.; Li, G. H.; Yang, F. H.; Yu, D. P., Luminescence emission originating from nitrogen doping of β−Ga2O3 nanowires. *Physical Review B* **2004,** *69* (7), 075304.
59. Sutter, E.; Ozturk, B.; Sutter, P., Selective growth of Ge nanowires by low-temperature thermal evaporation. *Nanotechnology* **2008,** *19* (43), 435607-435613.
60. Sutter, E.; Sutter, P., Axial Heterostructures with Phase-Controlled Metastable Segments via Post-Growth Reactions of Ge Nanowires. *Chemistry of Materials* **2019,** *31* (19), 8174-8181.

Table of Contents Graphic

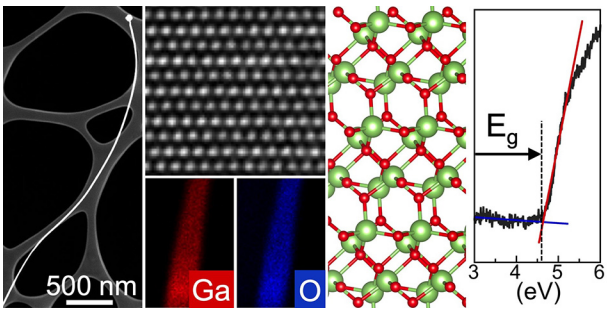

One-sentence description

Synthesis using a gallium sulfide precursor and Au or Ag catalysts produces ultrathin single-crystalline β-Ga_2O_3 nanowires at low substrate temperatures.